forum acusticum 2026
8-12 September · Graz, Austria

CHALLENGES IN MODELLING PLATE CONTACT CONDITIONS IN CROSS-LAMINATED TIMBER JUNCTIONS: A NUMERICAL-EXPERIMENTAL INVESTIGATION

Antonio Esposito[1], Stefan Schoenwald[1]

[1] *Swiss Federal Laboratories for Materials Science and Technology (Empa), Dübendorf, Switzerland*

Abstract

Existing numerical models reliably predict flanking sound transmission in cross-laminated timber (CLT) junctions when the stiffness of the connection approaches either the ideally rigid condition or that of an elastic layer interposed between plates. Nevertheless, it is still challenging to deterministically define coupling stiffness values for modelling the direct mechanical contact at the interface between plates. In this contribution, a numerical-experimental investigation is presented with the aim of highlighting fundamental issues for the determination of such coefficients. The vibration reduction index K_{ij} was measured for two configurations of a CLT L-junction mock-up. In the first case, the plates were in direct contact and connected by angle brackets. In the second, they were left in contact with each other, but without any fasteners. The comparison of finite element method simulations against experiments highlighted that the plates' coupling stiffness conditions are influenced by the simultaneous action of both the connectors and the static load on the junction. This is consistent with findings from previous studies on the effects of junction loading on flanking sound transmission. Implications of this study include the necessity of deriving an explicit relationship between the constraint/load conditions of the junction and the coupling stiffness coefficients at the plates' interface.

Keywords: *cross-laminated timber, finite element method, flanking sound transmission*

1. Introduction

Numerical models for predicting flanking sound transmission through cross-laminated timber (CLT) junctions are receiving increasing attention. Over the last years, modelling approaches have been introduced that achieved a satisfying degree of accuracy in predicting the vibration reduction index (K_{ij}) for junctions where the degree of rigidity of the connection approaches either the perfectly stiff condition or the elastic behaviour of resiliently decoupled junction [1], [2]. Nevertheless, in the context of finite element method (FEM) simulations, it may be useful to separately define stiffness coupling coefficients for transmission paths occurring through either the point connectors or the plates' contact interface, in cases where no decoupling layer is interposed. This might increase the versatility of FEM models, by accounting for a change in the number and location of connectors. Nevertheless, findings of a previous study have shown that the stiffening effects on the connection can be due to the simultaneous action of both vertical load and the application of point connectors [2]. Moreover, the increase of vertical loads has been also showed to exert a detrimental effect on the K_{ij} index as well as on the airborne sound insulation of CLT building junctions [3], [4]. On the other hand, it has been also demonstrated that flanking sound transmission in CLT wall-to-floor junctions can vary depending on the fastening configuration [5]. Based on the above, and building upon the findings of [2], this contribution provides experimental and numerical evidence of preliminary issues to consider for the definition of plates' coupling stiffness coefficients in FEM models. In particular, the experimental and numerical K_{ij} indices are reported for an L-junction mock-up, which was primarily constructed to validate the proposed modeling assumptions rather than for use in a real-world building application. In this specimen, two CLT plates are in direct contact with each other, either connected with two angle brackets or positioned in a manner that does not imply the use of point connectors. For each configuration, different modelling strategies are proposed to investigate the dependence of the plates' coupling stiffness coefficients on the constraint con-

***Corresponding author**: antonio.esposito@empa.ch.*

figuration of the connection. The paper is structured as follows: in Section 2, the theoretical background of the K_{ij} index measurements and of the performed FEM analyses is outlined; in Section 3, a description of the specimens as well as the numerical and experimental setups is provided; in Section 4, results are reported and discussed. Conclusions are summarised in Section 5.

2. Background and Theory

2.1. Vibration reduction index $K_{i,j}$

The Vibration Reduction Index K_{ij}, introduced in the ISO 12354-1:2017 standard [6], represents the attenuation of structure-borne sound transmission across a junction. It is frequency-dependent, expressed in decibels and defined as:

$$K_{ij} = \overline{D_{v,ij}} + 10lg\left(\frac{l_{ij}}{\sqrt{a_i a_j}}\right). \quad (1)$$

where $\overline{D_{v,ij}}$ is the direction-averaged velocity level difference between two elements, l_{ij} is the junction length and $a_{i,j}$ are the equivalent absorption lengths of the elements i and j. These are defined as [7]:

$$a = \frac{2.2\pi^2 S}{c_0 T_s}\sqrt{\frac{f_{ref}}{f}} \quad (2)$$

where T_s is the structural reverberation time and S is the surface area of the i^{th} or j^{th} element, f is the centre band frequency, f_{ref}, equal to 1 kHz, is the reference frequency and c_0 is the speed of sound in air.

2.2. FEM harmonic analysis

The equation of motion of a damped MDOF system, excited by an external harmonic force $\{\mathbf{F}\}$ reads:

$$[\mathbf{M}]\{\ddot{\mathbf{u}}\} + [\mathbf{K} + \mathbf{iH}]\{\mathbf{u}\} = \{\mathbf{F}\} \quad (3)$$

where $\{\ddot{\mathbf{u}}\} \in \mathbb{C}^n$ is the nodal acceleration vector, $\{\mathbf{u}\} \in \mathbb{C}^n$ is the nodal displacement vector, $[\mathbf{M}] \in \mathbb{R}^{n\times n}$ is the mass matrix, $[\mathbf{K}] \in \mathbb{R}^{n\times n}$ is the stiffness matrix of the system, $[\mathbf{H}]$ is the structural damping matrix of the system and $n \in \mathbb{R}$ is the number of degrees of freedom of the FEM model. For the purpose of the simulations presented herein, material-dependent constant structural damping coefficients η have been defined for each body of the system. To solve the harmonic response analyses, the full solution method was adopted, which solves equation (3) directly [8].

2.3. Structural coupling in FEM

In finite element analyses, it is frequently necessary to represent the mechanical interaction between connected components. Such connections often require the enforcement of kinematic relationships that govern the transfer of motion and load between deformable bodies [9]. For the CLT junctions analysed in this contribution, the mechanical contact at the plate-plate interface was modelled by connecting the two plates, modelled as shells, with MPC184 bushing joint elements, defined in Ansys Mechanical (Release 2025, R2). These elements provide a versatile framework for defining multipoint constraint equations, enabling the imposition of kinematic constraints between nodal degrees of freedom [8], [10]. The 'bushing' formulation within the MPC184 element is characterized by six degrees of freedom at each connected node, describing the complete relative motion between the two bodies. This motion comprises three translational and three rotational components, all evaluated within the joint reference coordinate system. The corresponding local force and moment components generated by the MPC184 bushing element can be expressed as follows [10]:

$$\left\{\frac{F}{M}\right\} = [K]\begin{Bmatrix} U_x \\ U_y \\ U_z \\ \theta_x \\ \theta_y \\ \theta_z \end{Bmatrix} + [C]\begin{Bmatrix} V_x \\ V_y \\ V_z \\ \Omega_x \\ \Omega_y \\ \Omega_z \end{Bmatrix} \quad (4)$$

where: $\{F\}$ and $\{M\}$ are the relative local force and moment, and $[K]$ and $[C]$ are the local stiffness and damping 6×6 matrices, relating the above forces to the relative nodal displacements (U_x, U_y, U_z), rotations $(\theta_x, \theta_y, \theta_z)$, velocities (V_x, V_y, V_z) and rotational velocities $(\Omega_x, \Omega_y, \Omega_z)$ in the constitutive law of the bushing. For the case presented in this contribution, the fully symmetric local stiffness matrix $[K]$ was defined using stiffness coeffcients. The definition of the damping matrix $[C]$ was neglected.

3. Materials and Methods

3.1. Description of the specimens

The investigations reported in this paper apply to the CLT L-junction mock-up depicted in Fig. 1. As visible in the figure, two CLT plates are connected to form an L-junction, with one plate positioned perpendicular to an edge of the other. In particular two configurations of the specimen are analysed:

- configuration **BC**, where 'B' stands for 'brackets' and 'C' stands for 'contact'. In this configuration, two angle brackets are used to connect the CLT plates, which are are in direct contact with each other, so that vibration transmission occurs through both the plate-bracket and plate-plate interfaces (Fig. 1a);
- configuration **C**, where 'C' stands for 'contact'. In this configuration, no brackets are used to connect CLT plates, ensuring that vibration transmission occurs only through the contact interface between plates (Fig. 1b).

3.2. Numerical models

The two CLT plates were characterised and validated experimentally in the modal domain as standalone systems, prior to the simulation of the global CLT

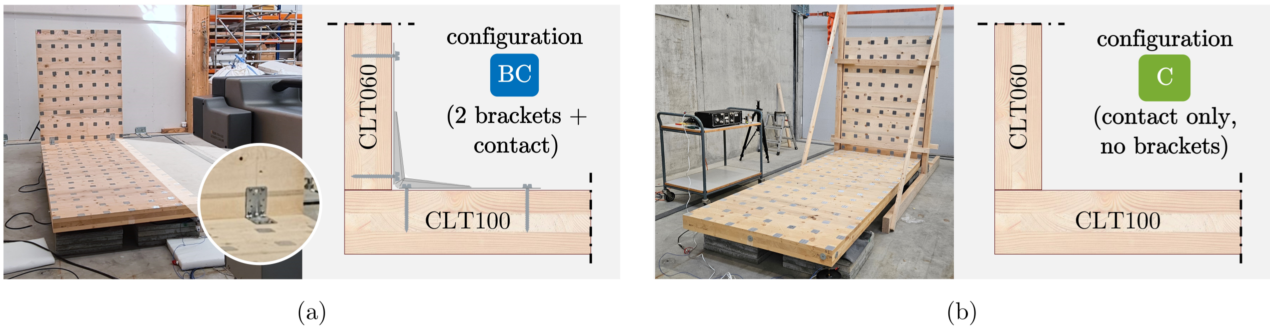

Figure 1: Experimental set-up of the L-junction mock-up: photos of the specimens and schematisation of the fastening systems and plates' contact interface of configurations (a) BC and (b) C.

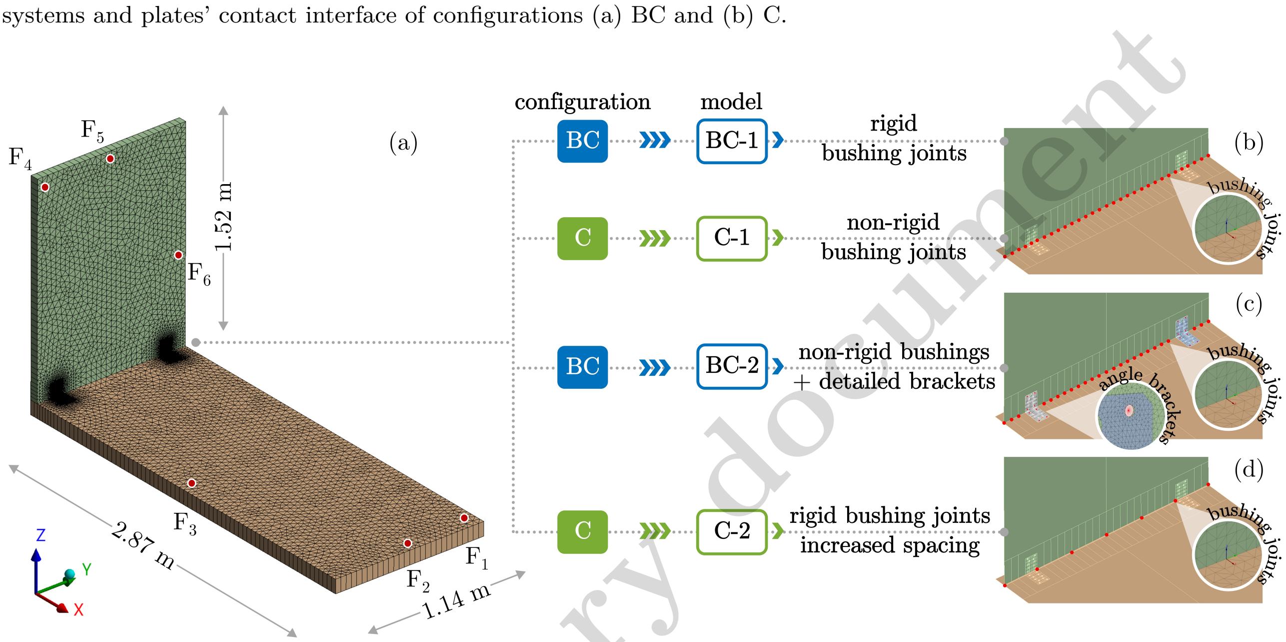

Figure 2: FEM model of the L-junction mock-up: (a) discretisation and excitation positions F_1 to F_6 used in the harmonic analyses. Modelling approaches of configurations BC and C using: (b) rigid bushing joints (BC-1) and non-rigid bushing joints (C-1), (c) non-rigid bushing joints with detailed connectors (BC-2) and (d) rigid bushing joints with increased spacing (C-2).

assembly. Please refer to [2] for more detailed information regarding their mechanical and geometrical properties. The plates are modelled in Ansys Mechanical (Release 2025, R2) as orthotropic shells with 6 degrees of freedom, including the orientation and the thickness of the plies in a layer-wise representation. Plates are meshed using quadratic triangular elements of 4 cm maximum size, as depicted in Fig. 2a. Full harmonic analyses are conducted in FEM for the L-junction in free-edge conditions. Plates are mechanically excited with transverse harmonic forces of 1 N amplitude at the points F_1 to F_6, as highlighted in Fig. 2a. As an output of the harmonic analyses, the normal surface velocities of the plates are mapped to the grid points used for the laser vibrometer measurements described in Section 3.3. The direction-averaged level difference $\overline{D_{v,ij}}$ was calculated by computing the surface average velocity levels of the plates for each excitation point. A logarithmic solution interval for the full harmonic analysis was defined, ranging from 562 Hz to 3548 Hz. The lower limit of the frequency range of interest was defined based on the modal overlap of the system, which exceeds unity starting from the 630 Hz third-octave frequency band, according to the experimental and numerical results reported in [2]. For each of the specimen configurations depicted in Fig. 1, the connection between the two plates is modelled using two different approaches, described in the following sections.

3.2.1. Model BC-1

One of the modelling strategies for configuration BC is reported here based on the results already presented in [2]. The contact at the plate-plate interface is modelled with the MPC184 elements defined in Section 2.3, by selecting node pairs along the shared edge of the two CLT plates at approximately 4 cm intervals (Fig. 2b). Local translational and rotational stiffness coupling coefficients were input into the stiffness matrix K_{BC} of Eq. (4), which resulted to be diagonal and symmetric, as follows:

$$K_{BC} = \begin{bmatrix} 1e^{10} & 0 & \cdots & 0 \\ 0 & 1e^{10} & \ddots & \vdots \\ \vdots & \ddots & \ddots & 0 \\ 0 & \cdots & 0 & 1e^{10} \end{bmatrix}_{6\times 6} \tag{5}$$

where the first three diagonal elements represent the translational stiffnesses (N·m) relating the nodal relative forces to the relative nodal displacements (U_x, U_y, U_z) and the second third entries are the rotational stiffnesses (N·m/rad) relating the nodal relative moments to the relative rotations $(\theta_x, \theta_y, \theta_z)$ around the x, y and z axes. The choice of such coefficients is based on the numerical investigations reported in [2], where it has been demonstrated that, for the specimen in question, the connection mechanics approach that of an infinitely rigid bushing.

3.2.2. Model C-1

Similarly to the model BC-1, the plate-plate interface in configuration C is hereby modelled by applying MPC184 elements to nodal pairs along the common edge of the plates, keeping the same spacing of approximately 4 cm. Due to the non-rigid behaviour of the connection, the entries of the K_C matrix are retrieved with a parameter estimation procedure based on the experimental data resulting from the vibrometry measurements described in Section 3.3. The coupling stiffness K_C matrix is populated as follows:

$$K_C = \begin{bmatrix} 2e^6 & 0 & & \cdots & & 0 \\ 0 & 1e^6 & & & & \\ & & 1e^6 & \ddots & & \vdots \\ \vdots & & \ddots & 1e^5 & & \\ & & & & 1e^3 & 0 \\ 0 & & \cdots & & 0 & 1e^5 \end{bmatrix}. \tag{6}$$

3.2.3. Model BC-2

In addition to the approach used in the model BC-1, the configuration BC is replicated by modelling the plate-plate and the plate-bracket interface separately. The former is simulated by using the same MPC184 stiffness values utilised for the model C-1, but excluding the node pairs falling in close proximity to the brackets, as depicted in Fig. 2c. Connectors are then simulated by introducing a detailed model of a steel angle bracket, already validated experimentally in [2]. The fastening at the plate-bracket interface was modelled by defining rigid multi-point constraint (MPC) joints at each screw position. In particular the nodes along the edges of the bracket screw holes and the corresponding nodes projected onto the adjacent plates are linked and constrained to have the same solution as a single independent node located at the origin of the joint reference system (Fig. 2c) [10].

3.2.4. Model C-2

An alternative modelling strategy for configuration C is proposed hereby, obtained by using the stiffness entries as in Eq. (5), which were originally adopted to model configuration BC, and increasing the spacing between the node pairs of the MPC184 bushing joints to approximately 19 cm, as depicted in Fig. 2d. In this case, the aim is to model the reduction in vibration transmission resulting from the decreased stiffness of the connection, assuming that the contact area between the CLT plates, which is inherently limited by surface irregularities at the interface, is further diminished by the reduced stiffness of the connection.

3.3. Experimental setup

The numerical models above were validated with reference to the experimental data obtained from the laser Doppler vibrometry measurements, published in [2]. The experimental setup of these measurements is summarised hereby for the sake of completeness.

To emulate the free boundary conditions of the specimen, the L-junction mock-up was resting on four air jacks, located close to the corners of the horizontal plate, the internal air pressure of which has been kept constant during the measurements. Each plate was dynamically excited with a shaker emitting a sine sweep signal. For each plate, three different excitation positions were set up, according to the schematization of the numerical model depicted in Fig. 2a. Normal surface velocities were acquired with a Polytec PSV-400 scanning vibrometer pointing normally to the plates, over a 17×7 points regular grid for the horizontal plate, and over a 9×7 points grid for the vertical plate. Data were acquired within the 1 Hz - 5.8 kHz frequency interval with a resolution of 62.5 mHz.

4. Results and Discussion

In this section, results are reported and discussed by comparing the experimental and numerical vibration reduction indexes K_{ij} for both configurations BC and C. Data are presented in third-octave bands, ranging from 630 Hz to 3150 Hz. In particular, to facilitate comparison between the various dataset pairs, the following indicators have been used as a reference:

- $\overline{|\Delta K_{ij}|}$, absolute value difference between the K_{ij} of the dataset pairs, averaged over the 630 Hz-3150 Hz frequency range;
- $max(|\Delta K_{ij}|)$, maximum absolute value difference between the K_{ij} of the dataset pairs;
- $|\Delta K_{ij,high}|$, absolute value difference between the single number rating $K_{ij,high}$, defined in the ISO 10848-1:2017 standard [7], of the dataset pairs.

Starting from the comparison between the measured data of configurations BC and C, reported in Fig. 3 and Table 1, it is observable that configuration C shows higher overall K_{ij} values, with a $\overline{|\Delta K_{ij}|}$ 5 dB

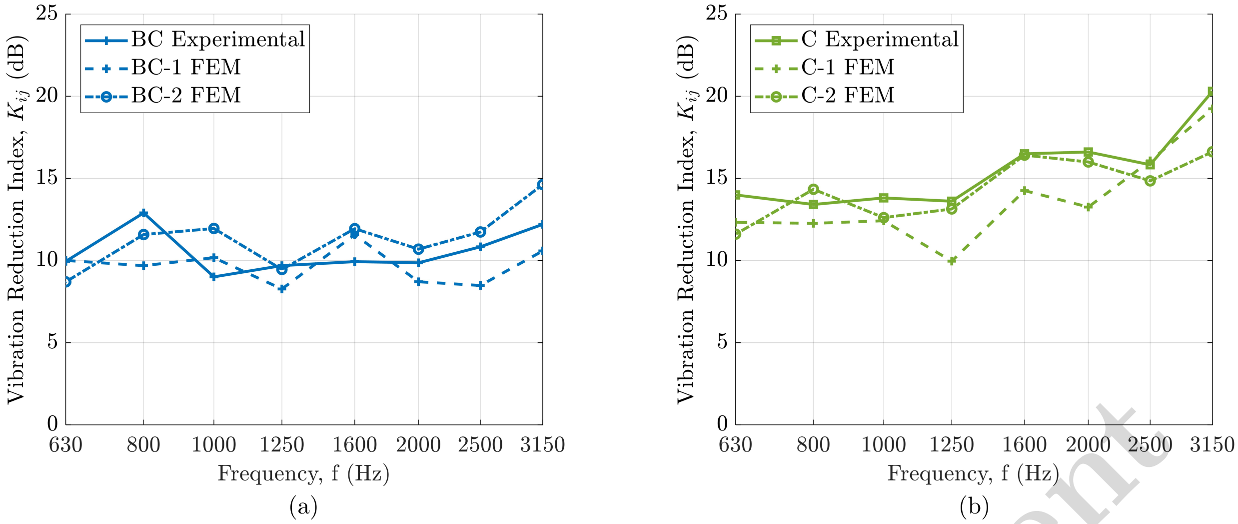

Figure 3: Comparison between the experimental and numerical vibration reduction index K_{ij} for (a) configuration BC and (b) configuration C.

Table 1: Overview of the K_{ij} comparison between numerical (BC-1, BC-2, C-1, C-2) and experimental (BC, C) datasets. The frequency averaged absolute value differences $\overline{|\Delta K_{ij}|}$ between the K_{ij} of each dataset pair are reported with the relative maximum value $max(|\Delta K_{ij}|)$. Additionally, the single number rating $|K_{ij,\text{high}}|$ values [7] are listed for each dataset pair together with their absolute value difference $|\Delta K_{ij,\text{high}}|$.

Dataset 1	Dataset 2	$\overline{\lvert\Delta K_{ij}\rvert}$ (dB)	max($\lvert\Delta K_{ij}\rvert$) (dB)	$K_{ij,\text{high}}$ (dB)		$\lvert\Delta K_{ij,\text{high}}\rvert$ (dB)
				Dataset 1	Dataset 2	
BC	C	5.0	8.1	10.5	16.6	6.1
BC	BC-1	1.6	3.2	10.5	9.5	1.0
BC	BC-2	1.5	2.9	10.5	11.7	1.2
C	C-1	1.8	3.6	16.6	14.6	2.0
C	C-2	1.3	3.7	16.6	15.4	1.2

higher than configuration BC and a $max(|\Delta K_{ij}|)$ of 8.1 dB. This trend is confirmed by the $|\Delta K_{ij,high}|$ value, equal to 6.1 dB. This quantifies the higher vibration transmission occurring across the junction in configuration BC. This difference is particularly evident at high frequencies where, in the configuration BC, a flattening of the K_{ij} curve is observed starting from 1.25 kHz. This highlights the stiffening action of the connectors, which, when combined with the mechanical contact at the plate-plate interface in this specific case, produces effects that are comparable to the application of a static load to the junction [3].

In light of the above, by comparing the two experimental datasets, BC and C, with the results of the respective numerical models, BC-1 and C-1, it is possible to make a preliminary evaluation of the effect of junction stiffening on the coupling stiffness coefficients used in the bushings MPC184. As observable in Fig. 3 and Table 1, the $\overline{|\Delta K_{ij}|}$, calculated between the model BC-1 and the respective experimental data of configuration BC, is 1.6 dB, with a $max(|\Delta K_{ij}|)$ of 3.2 dB and a difference in terms of $K_{ij,high}$ equal to 1 dB. A similarly good correlation emerges from a comparison of the experimental data of configuration C to the results of model C-1, with a $\overline{|\Delta K_{ij}|}$ of 1.8 dB, a $max(|\Delta K_{ij}|)$ of 3.6 dB and a $|\Delta K_{ij,high}|$ equal to 2 dB. These preliminary assessments suggest the possibility of establishing an explicit relationship between the load/constraint conditions of the junction and the coupling stiffness coefficients between the plates. This might allow to bypass the detailed modelling of connectors, reducing the computational costs of predictive models for the evaluation of the K_{ij} index. Furthermore, a good correlation is observable between the numerical results of the model BC-2 and the experimental K_{ij} of configuration BC, with a $\overline{|\Delta K_{ij}|}$ of 1.5 dB, a $max(|\Delta K_{ij}|)$ of 2.9 dB and a $|\Delta K_{ij,high}|$ equal to 1.2 dB. In light of this, the use of the stiffness coupling coefficients of the model C-1, combined with the detailed model of the brackets, may suggest that considerable scope exists for enhancing the versatility of FEM models of more complicated CLT junctions, by simulating the mechanics at the plate-plate and plate-connectors interfaces separately.

Finally, a comparison between the results of the model C-2 and the measured data of configuration C ($\overline{|\Delta K_{ij}|} = 1.3\,\text{dB}$, $max(|\Delta K_{ij}|) = 3.7\,\text{dB}$, $\overline{|\Delta K_{ij,high}|} = 1.2\,\text{dB}$) highlights the potential of a further modelling strategy, based on the use of rigid MPC184 bushings with increased interspacing. The possibility of establishing an explicit relationship, governing the distance between bushings in relation to the wavelengths involved in the vibration transmission, remains to be ascertained. This is because the effective interaction between the CLT plates depends on the interface contact area, which is influenced by the surface roughness, the applied normal load and the mechanical connectors.

5. Conclusion

In this contribution, two different configurations of a CLT L-junction mock-up were tested: one where the two plates were in direct contact and connected with two steel angle brackets; another without connectors, in order to analyse the vibration transmission across the junction due to only mechanical contact between the two plates. For each of these configurations, two different FEM modelling strategies were proposed and validated in terms of K_{ij}. The aim was to investigate possible preliminary issues for the definition of coupling stiffness coefficients in the FEM simulation of the mechanical contact at the plate-plate interface.

The analysis of the K_{ij} indices measured on the two configurations of the specimen revealed that the stiffening action of connectors, in combination with the static loading due to the direct contact between the plates, results in a flatter high-frequency K_{ij} curve than the less rigid configuration. This effect has been reproduced by validating two different numerical models, where the connection stiffness was simulated using MPC184 bushings applied at regularly spaced node pairs along the plates' common edge. In particular, according to the outcomes of a previous study [2], the configuration with brackets was modelled by using rigid bushing stiffness values. Conversely, for the configuration without brackets, non-rigid bushing stiffness values were determined through a parameter estimation procedure that remains under development. Although preliminary, these results suggest that there may be scope for the determination of an explicit relationship between the constraint/load conditions of the junction and the coupling stiffness coefficients between CLT plates.

Furthermore, the reliability of such values was proved with the experimental validation of a further numerical model of the stiffer junction. In this simulation, alongside the use of the non-rigid bushings, a detailed model of the two brackets was introduced to simulate the connection at the plate-bracket interface. This analysis provides, as a preliminary matter, enhanced versatility to the FEM models of CLT junctions, by simulating the plate-plate and the plate-connector interfaces separately. Finally, an alternative approach was preliminarily tested for modelling the contact at the plate-plate interface. In particular, nodal rigid bushings were used in a reduced quantity, by increasing their relative spacing along the common edge of the plates. The validation of such model provided new input for the possible definition of a relationship that governs the distance between nodal bushings as a function of the wavelengths involved in the vibration transmission mechanisms of the system. Nevertheless, this question is still under investigation.

References

[1] S. Moons, R. Lanoye, and E. P. Reynders, "Prediction of flanking sound transmission through cross laminated timber junctions with resilient interlayers," *Applied Acoustics*, vol. 228, p. 110 317, 2025.

[2] A. Esposito, S. Vallely, B. Kurent, and S. Schoenwald, "Finite element modelling of bracket-connected cross-laminated timber plates to calculate vibration reduction indices," *Acta Acustica*, vol. 10, no. 39, 2026.

[3] V. P. Possenti, C. Crispin, A. Dijckmans, and L. Barbaresi, "Load effects in flanking transmission of CLT structures with resilient interlayer," in *Proc. of the 11th Convention of the European Acoustics Association Forum Acusticum / EuroNoise 2025*, Málaga, Spain, 2025, pp. 611–617.

[4] E. Nilsson, S. Ménard, D. Bard, and K. Hagberg, "Effects of building height on the sound transmission in cross-laminated timber buildings – airborne sound insulation," *Building and Environment*, vol. 229, p. 109 985, 2023.

[5] F. Morandi, S. D. Cesaris, M. Garai, and L. Barbaresi, "Measurement of flanking transmission for the characterisation and classification of cross laminated timber junctions," *Applied Acoustics*, vol. 141, pp. 213–222, 2018.

[6] ISO 12354-1:2017, "Building acoustics — Estimation of acoustic performance of buildings from the performance of elements," International Organization for Standardization, Geneva, CH, Standard, 2017.

[7] ISO 10848-1:2017, "Acoustics — Laboratory and field measurement of flanking transmission for airborne, impact and building service equipment sound between adjoining rooms - Part 1: Frame document," International Organization for Standardization, Geneva, CH, Standard, 2017.

[8] Ansys® Academic Research Mechanical APDL Help System, *Theory reference*, ANSYS, Inc., 2025.

[9] Ansys® Academic Research Mechanical APDL Help System, *Element reference*, ANSYS, Inc., 2026.

[10] Ansys® Academic Research Mechanical Application Help System, *Mechanical user's guide*, ANSYS, Inc., 2026.